# Comparison of Rotor Structural Loads Calculated Using Comprehensive Analysis

Hyeonsoo Yeo

Aeroflightdynamics Directorate (AMRDEC)
U.S. Army Research, Development, and Engineering Command
Ames Research Center, Moffett Field, California

Wayne Johnson

Flight Vehicle Research and Technology Division
NASA Ames Research Center
Moffett Field, California

## Abstract

Blade flap and chord bending and torsion moments are investigated for six rotors operating at transition and high speed: H-34 in flight and wind tunnel, SA 330 (research Puma), SA 349/2, UH-60A full-scale, and BO-105 model (HART-I). The measured data from flight and wind tunnel tests are compared with calculations obtained using the comprehensive analysis CAMRAD II. The calculations were made using two free wake models: rolled-up and multiple-trailer with consolidation models. At transition speed, there is fair to good agreement for the flap and chord bending moments between the test data and analysis for the H-34, research Puma, and SA 349/2. Torsion moment correlation, in general, is fair to good for all the rotors investigated. Better flap bending and torsion moment correlation is obtained for the UH-60A and BO-105 rotors by using the multiple-trailer with consolidation wake model. In the high speed condition, the analysis shows generally better correlation in magnitude than in phase for the flap bending and torsion moments. However, a significant underprediction of chord bending moment is observed for the research Puma and UH-60A. The poor chord bending moment correlation appears to be caused by the airloads model, not the structural dynamics.

## Nomenclature

| | |
|---|---|
| $c$ | nominal blade chord |
| $C_T$ | rotor thrust coefficient |
| $M$ | Mach number |
| $N_b$ | number of blades |
| $r$ | blade radial station |
| $R$ | blade radius |
| $\alpha_{TPP}$ | tip path plane tilt angle, positive forward |
| $\mu$ | advance ratio |
| $\sigma$ | solidity |
| $\Omega$ | rotor rotational speed |

## Introduction

The accurate prediction of rotor loads and vibration remains a difficult problem for helicopter design. Typically, helicopters encounter high vibration in two different speed regimes: transition and high speed. The rotor blade aerodynamic environment in transition is characterized by blade-vortex interactions, and in high speed by compressibility and negative loading on the advancing side. The ability to accurately predict the rotor blade loads for these two flight regimes is essential for the design of future rotorcraft.

*Presented at the 31st European Rotorcraft Forum, Florence, Italy, September 13-15, 2005.*

For the past several decades a number of flight and wind tunnel tests have been conducted to understand the nature of airloads acting on the rotor blade and structural loads due to aerodynamic loading [1–6]. These extensive flight and wind tunnel data sets provide a valuable resource that can be used to evaluate comprehensive codes' accuracy and reliability and to develop better methodologies to simulate the rotor dynamic response.

Analyses need to provide consistently good predictions for various rotors and flight conditions in order to be used for design work. The first step to obtain better prediction is to understand the deficiencies of the current analyses. This can be achieved by comparing calculations with flight and wind tunnel measurements for different rotors. Once the deficiencies are identified, effort can be made to improve the methodology.

Reference 7 compared structural measurements from flight and wind tunnel tests of a number of full-scale rotors at a high speed condition. It was concluded that the similar load behavior observed among several rotors provides a good test for theoretical methods. The present study examines the blade structural loads at both low and high speeds and compares the analytical methods with experimental measurements.

Reference 8 compared calculated airloads with measured data for the same rotors considered in the present paper.

The calculated blade section normal force showed fair to good correlation at low speed. However, the same analysis showed, in general, poor correlation at high speed. As a continuation of the work in Ref. 8, this paper focuses on flap and chord bending and torsion moment correlation.

The purpose of the present study is threefold: 1) understand the similarities and differences in blade loads among the measurements as well as calculations, 2) assess the accuracy and reliability of a comprehensive code in the calculation of blade loads and investigate the deficiencies of the current analysis and key elements to improve the correlation, and 3) carry out calculations with various wake models and identify important wake parameters for the loads calculation. The calculations were performed using the comprehensive analysis CAMRAD II [9].

## Test Data

Flight and wind tunnel test cases from various rotors [1–6] have been carefully selected so that they represent similar test conditions. Figure 1 and Table 1 show the thrust and advance ratio considered and some of the rotor parameters. The thrust coefficient values range from $C_T/\sigma$ = 0.057 to 0.079, and the advance ratios are in the range of $\mu$ = 0.129 to 0.15 at transition, and $\mu$ = 0.361 to 0.39 at high speed.

The flight [1] and wind tunnel [2] tests of an H-34 helicopter have long been a standard for rotor loads correlation. The blade flap and chord bending and torsion moment data for the H-34 in flight were measured at six radial stations (r/R = 0.15, 0.275, 0.375, 0.45, 0.575, and 0.65), three radial stations (r/R = 0.15, 0.375, and 0.575), and two radial stations (r/R = 0.15, and 0.5), respectively, and were averaged over three consecutive revolutions. Time history data are available with a 15 degree azimuthal step. The structural loads data for the H-34 in the wind tunnel were were averaged over ten revolutions. Harmonic data (up to 10/rev) are available at r/R = 0.375 and 0.65, and time history data are available at the other radial stations with a 5 degree azimuthal step.

The research Puma (SA 330) data were obtained using a modified swept-tip blade rather than the standard rectangular Puma blade [3]. A single revolution of data was taken for each test point, therefore, there is no averaging of data. High resolution data (up to 256/rev) are available, but the data used in this paper have 3 degree azimuthal resolution.

The SA 349/2 flight data were obtained from an upgraded Gazelle helicopter with three research Grande Vitesse (GV) blades [4]. Data from each of the strain gauges were acquired over a period of six consecutive rotor revolutions and then averaged. Harmonic data are available up to 10/rev.

Test data with the UH-60A were obtained from the NASA/Army UH-60A Airloads Program [5]. For this study, a single revolution of data was used from each test point. The data have 7.5 degree azimuthal resolution.

The BO-105 data were obtained from the Higher-harmonic Acoustics Rotor Test (HART-I) program using a 40% Mach-scaled hingeless BO-105 main rotor blade [6]. The objective of the test was to demonstrate the reduction of blade-vortex interactions (BVI) noise in the descending flights using higher-harmonic controls (HHC). The data set used for the current study is a baseline case without higher-harmonic pitch control inputs. The shaft angle for this condition was 5.3 degree aft (4.2 degree aft when corrected for tunnel wall effects). The structural loads data were averaged over 32 revolutions and filtered to 8 harmonics.

Figure 2 shows the blade planforms for the five rotors, along with the location of the airfoils used and the structural loads measurements.

## CAMRAD II Modeling

### Rotor Trim Procedure

The H-34 in flight and wind tunnel, research Puma and UH-60A Black Hawk in flight, and model-scale BO-105 in wind tunnel were modeled in CAMRAD II as isolated rotors. The trim solution for the H-34 in flight and wind tunnel and the research Puma in flight solved for the controls that produced rotor thrust and first harmonic flapping to match the measured values, with the rotor shaft angle of attack fixed at the measured values. The trim solution for the UH-60A in flight and BO-105 in wind tunnel solved for the controls that produced rotor thrust and shaft pitch and roll moments to match the measured values, with the rotor shaft angle of attack fixed at the measured values.

The SA 349/2 in flight was analyzed as a complete aircraft, with the Fenestron tail rotor modeled as an auxiliary anti-torque force. The trim solution for the SA 349/2 in flight solved for the controls and aircraft attitudes that produced zero total force and moment on the aircraft, with zero sideslip angle.

### Rotor Wake Model

The wake analysis in CAMRAD II calculates the rotor nonuniform induced-velocity using free wake geometry.

The concentrated tip vortices are the key features of the rotor wake, important for performance, airloads, structural loads, vibration, and noise calculations. The formation of the tip vortices is modeled in CAMRAD II, not calculated from first principles. Two cases are examined here: a rolled-up model and a multiple-trailer with consolidation model. Because of its simplicity and efficiency, the rolled-up model has long been used for helicopter rotors. The multiple-trailer model has also been available, and with the consolidation feature has been applied recently with success to tiltrotor and helicopter airloads calculations [8, 10].

The rolled-up wake model is based on the assumption that a tip vortex forms at the blade tip. The bound circulation can have the same sign all along the blade span, or there may be two bound circulation peaks (inboard and outboard peaks of opposite sign). These are the single-peak and dual-peak cases. For the current study, the single-peak model was used for the low speed conditions, and the dual-peak model was used for the high speed conditions.

The multiple-trailer model has the far wake trailed vorticity divided into several spanwise panels, to provide more detailed structure for the inboard vorticity, with consolidation of trailed lines in the wake geometry to model the rollup process. This model has a discrete trailed vortex line emanating from each of the aerodynamic panel edges. The calculation of the free wake geometry includes the distortion of all of these trailed lines. With multiple far wake trailed vorticity panels, the trailed lines at the aerodynamic panel edges can be consolidated into rolled-up lines, using the trailed vorticity moment to scale the rate of roll-up. The trailed vorticity is partitioned into sets of adjacent lines that have the same sign (bound circulation increasing or decreasing). It is assumed that all the vorticity in a set eventually rolls up into a single vortex, located at the centroid of the original vorticity distribution.

Reference 9 has more detailed description on the wake modeling in CAMRAD II.

## Blade Properties

For the accurate calculation of structural loads, it is important to obtain accurate blade structural properties. The structural properties for the H-34, research Puma, and SA 349/2 were obtained from Refs. 2, 3, and 4, respectively. The UH-60A blade properties were obtained from the input database, which has been developed and refined over the past years and showed good performance correlation [11]. The blade properties for the model-scale BO-105 blade were obtained from the blade manufacturer and were modified to match the measured non-rotating natural frequencies. In addition, adjustments were made to the elastic axis and c.g. offset of the BO-105 blade to obtain better airload correlation.

## Results and Discussion

The calculated blade flap and chord bending and torsion moments were compared with the flight and wind tunnel measurements. The calculations have been conducted with the identical analysis options for all rotors (Ref. 12).

### Blade Natural Frequencies

The blade natural frequencies were calculated from 40% to 110% of the nominal rotor speed and the results are shown in Fig. 3. The first flap frequencies of the articulated rotors (H-34, research Puma, SA 349/2, and UH-60A) range from about 1.02 to 1.04/rev. The first flap mode frequency of the model-scale BO-105 rotor, which is a hingeless rotor, is higher than those of the articulated rotors. The second flap mode frequencies range from about 2.7 to 2.9/rev, and this is the dominant vibratory flap bending mode for these aircraft. The second flap frequency of the research Puma is closest to 3/rev and that of the H-34 is furthest from 3/rev.

All the first chord mode frequencies are below 1/rev. Again, the first chord mode frequency of the model-scale BO-105 rotor, which is a hingeless rotor, is higher than those of the articulated rotors. Considerably more variation is seen in the second chord mode frequencies than was seen in the second flap mode modes.

The first torsion frequency of the H-34 is quite high (above 6/rev). The other rotors show first torsion mode frequencies that range from 4/rev to 5/rev.

### Flap Bending Moment Correlation

The measured flap bending moment data from flight and wind tunnel tests were compared with calculations obtained using the comprehensive analysis CAMRAD II.

Figure 4 shows non-dimensional oscillatory flap bending moments of the H-34, research Puma, SA 349/2, UH-60A Black Hawk, and BO-105 rotors at low speed. Steady values were removed from both test data and analysis. The flap bending moments are shown in the non-dimensional form

$$C_{FM}/\sigma = \frac{M_F}{\rho N_b c \Omega^2 R^4}$$

where $M_F$ is the flap bending moment.

Calculations were made using two wake models: a rolled-up and a multiple-trailer wake with consolidation. The analysis results were compared with measured data near mid-span. The analysis with the rolled-up wake model shows, in general, good correlation in both magnitude and phase for the H-34, research Puma, and SA 349/2. The calculated flap bending moments differ significantly from the measurements for the UH-60A and BO-105.

Better correlation was obtained for the UH-60A by using the multiple-trailer with consolidation wake model. For the BO-105, although the multiple-trailer with consolidation wake model shows a slight improvement on the waveform in the second and third quadrants, the analysis shows poor correlation.

Figure 5 shows non-dimensional oscillatory flap bending moments at high speed. The analysis shows fair correlation for the H-34. The research Puma data show the dominant 3/rev loading and the analysis captures the strong 3/rev loading reasonably well. In general, the correlation for the SA 349/2 is is fair to good. For the UH-60A, the calculated flap bending moments show fair correlation on magnitude, but the phase differs significantly from the measurements. Except for the SA 349/2, the multiple-trailer with consolidation model has a small influence on the prediction of flap bending moment at high speed.

**Chord Bending Moment Correlation**

Figures 6 and 7 show non-dimensional oscillatory chord bending moment correlation at low and high speed, respectively. Steady values were removed from both test data and analysis.

At low speed, the analysis shows fair to good correlation for the H-34 and SA 349/2. However, a significant difference between the analysis and measured data was observed for the UH-60A and BO-105, underpredicting the peak-to-peak magnitude. For the research Puma, correlation is good on the retreating side but poor on the advancing side. In general, the influence of wake modeling has a small influence on the prediction of chord bending moment.

At high speed, the analysis shows good correlation for the H-34. For the SA 349/2, correlation is good on the retreating side but poor on the advancing side. Although the test show the dominant 4/rev loading for the research Puma and UH-60A, the analysis was not able to capture the strong 4/rev response, significantly underpredicting the magnitude.

The chord bending moment correlation will be further discussed below.

**Torsion Moment Correlation**

Figures 8 and 9 show non-dimensional oscillatory torsion moment correlation at low and high speed, respectively. Steady values were removed from both test data and analysis. Most of the first torsion frequencies are between 4/rev and 5/rev for the rotors investigated. However, torsion moments are not dominated by 4/rev or 5/rev. Although the pitching moment correlation, in general, was poor as shown in Ref. 8, the analysis shows fair to good torsion moment correlation at both low and high speeds. Because there is a strong modal coupling between the first torsion, third flap, and second chord modes, the normal force contribution to the torsion moments appears to be important. Better correlation was obtained for the UH-60A and BO-105 by using the multiple-trailer with consolidation wake model at low speed. Because the multiple-trailer with consolidation wake model improved the airloads on the advancing side of the UH-60A and BO-105 rotors at low speed, it is consistent that better torsion moment correlation was obtained on the advancing side. A phase difference was still observed in the first and second quadrants for the research Puma and UH-60A.

At high speed, the measured torsion moment shows a strong 1/rev response, which the analysis captures reasonably well. However, a 30 degree phase difference is observed for the SA 349/2 and UH-60A.

**Vibratory Flap Bending Moment Correlation**

Figure 10 shows the vibratory flap bending moments at low speed. Steady, 1/rev, and 2/rev harmonics have been removed from the test data and analyses for the H-34, research Puma, UH-60A, and BO-105. Steady and 1/rev harmonics have been removed for the 3-bladed SA 349/2. The harmonics retained are the vibratory loads that are transmitted through the shaft to the fuselage and produce vibration at $N_b$ per rev.

Both the rolled-up and multiple-trailer with consolidation wake models show fair to good correlation for the H-34, research Puma, and SA 349/2. The rolled-up wake model overpredicts the magnitude for the UH-60A. The multiple-trailer with consolidation model tends to reduce the magnitude and thus shows better correlation. Both the rolled-up and multiple-trailer with consolidation wake models show poor to fair correlation for the BO-105.

Figure 11 shows the vibratory flap bending moments at high speed. The analysis shows fair to good correlation for the H-34, research Puma, and SA 349/2. The correlation for the UH-60A is poor. Although the magnitude was reasonably captured, there is a significant phase error.

### Further Examination of Chord Bending Moment

To understand the poor correlation of the chord bending moment for some of the rotors investigated, the effects of chord stiffness and lag damping were evaluated by looking at arbitrary changes of those quantities. This investigation was conducted for the UH-60A in the high speed condition. Figure 12(a) shows that the effect of chord stiffness on the chord bending moment is small. Because the analysis significantly underpredicted the dominant 4/rev response, the chord stiffness values were reduced by 20% each from the baseline values to move the first chord mode. The first chord frequency of the 60% chord stiffness case was 4.04/rev. However, even in that case there was no strong 4/rev response observed. Figure 12(a) shows that the effect of lag damping on the chord bending moment is small. Linear damper model was used in the current investigation. Although not shown here, a non-linear lag damper model had a very small influence on the chord bending moment at 50% radius. Damping value is important when the natural frequency is close to resonance. Thus, even the zero damping did not change the chord bending moment with the baseline chord stiffness.

The rotor blade structural response was calculated using prescribed measured airloads. The pressure data were integrated to obtain normal and chord force and pitching moment. Thus, pressure chord force does not include viscous drag. In this way, the rotor structural dynamics problem can be isolated from the rotor aerodynamics problem. Figure 12(c) shows that the chord bending moment was significantly improved by using the measured airloads, although the discrepancy still exists on the front of the rotor disk. Better results can be obtained with measured lag damper force (Ref. 13).

The poor correlation of the chord bending moment appears to be caused by the airloads model, not the structural dynamics.

## Conclusions

Blade flap and chord bending and torsion moments were investigated for various rotors operating at transition and high speeds: H-34 in flight and wind tunnel, SA 330 (research Puma), SA 349/2, UH-60A full-scale and BO-105 model (HART-I). The H-34, research Puma, SA 349/2, UH-60A data represent steady, level flight conditions and the BO-105 data represent a descending flight condition. Measured data from flight and wind tunnel tests were compared with calculations obtained using the comprehensive analysis CAMRAD II.

From this study the following conclusions were obtained:

### Low Speed

1. The analysis with a rolled-up wake model shows good flap bending moment correlation for the H-34, research Puma, and SA 349/2. The calculated flap bending moments differ significantly from the measurements for the UH-60A and BO-105.

2. Better flap bending moment correlation is obtained for the UH-60A by using the multiple-trailer with consolidation wake model. However, differences remain between the measurement and analysis.

3. Although the multiple-trailer with consolidation wake model shows good correlation on the normal force for the BO-105 (Ref. 8), the same analysis shows poor correlation on the flap bending moment.

4. The analysis shows fair to good chord bending moment correlation for the H-34, and SA 349/2, but significantly underpredicts peak-to-peak magnitude for the UH-60A and BO-105. For the research Puma, correlation is good only on the retreating side.

5. The wake modeling has a small influence on the calculation of chord bending moment.

6. The torsion moment correlation is quite satisfactory for all the rotors investigated, although aerodynamic pitching moment correlation, in general, was poor (Ref. 8). Better correlation is obtained for the UH-60A and BO-105 by using the multiple-trailer with consolidation wake model.

### High Speed

1. Measured vibratory bending moments show strong 3/rev response at both low and high speed and those are dominated by the second flap bending mode.

2. The analysis shows fair to good oscillatory flap bending moment correlation for the H-34, research Puma, and SA 349/2 and poor phase correlation for the UH-60A.

3. The chord bending moment correlation is good for the H-34 and fair for the SA 349/2. The calculated chord bending moments differ significantly from the measurements for the research Puma and UH-60A.

4. The effect of the chord bending stiffness and lag damping value changes on the chord bending moment is small. The poor chord bending moment correlation appears to be caused by the airloads model, not the structure dynamics.

5. The measured torsion moment shows a strong 1/rev response, which the analysis captures reasonably well. However, a 30 degree phase difference is observed for the SA 349/2 and UH-60A.

## References


[1] Scheiman, J., "A Tabulation of Helicopter Rotor-Blade Differential Pressures, Stresses, and Motions as Measured in Flight," NASA TM X-952, 1964.

[2] Rabbott, J. P. Jr., Lizak, A. A., and Paglino, V. M., "A Presentation of Measured and Calculated Full-Scale Rotor Blade Aerodynamic and Structural Loads," USAAVLABS TR 66-31, 1966.

[3] Bousman, W. G., Young, C., Gilbert, N. E., Strawn, R. C., Miller, J. V., Maier, T. H., Costes, M., and Beaumier, P., "A Comparison of Lifting-Line and CFD Methods with Flight Test Data from a Research Puma Helicopter," NASA TM 110421, October 1996.

[4] Heffernan, R. M., and Gaubert, M., "Structural and Aerodynamic Loads and Performance Measurements of an SA 349/2 Helicopter with an Advanced Geometry Rotor," NASA TM 88370, November 1986.

[5] Kufeld, R. M., Balough, D. L., Cross, J. L., Studebaker, K. F., Jennison, C. D., and Bousman, W. G., "Flight Testing of the UH-60A Airloads Aircraft," American Helicopter Society 50th Annual Forum Proceedings, Washington D.C., May 1994.

[6] Splettstoesser, W. R., Heller, H., Mercker, E., Preisser, J. S., and Yu, Y. H., "The HART Programme, a Quadrilateral Cooperative Research Effort," American Helicopter Society 51st Annual Forum Proceedings, Ft. Worth, TX, May 1995.

[7] Bousman, W. G., "The Response of Helicopter Rotors to Vibratory Airloads," *Journal of the American Helicopter Society*, Vol. 35, No. 4, October 1999.

[8] Yeo, H., and Johnson, W., "Assessment of Comprehensive Analysis Calculation of Airloads on Helicopter Rotors," American Helicopter Society 4th Decennial Specialists' Conference on Aeromechanics, San Francisco, CA, January 2004.

[9] Johnson, W., "Technology Drivers in the Development of CAMRAD II," American Helicopter Society Aeromechanics Specialist Meeting, San Francisco, CA, January 1994.

[10] Johnson, W., "Influence of Wake Models on Calculated Tiltrotor Aerodynamics," American Helicopter Society Aerodynamics, Acoustics , and Test and Evaluation Technical Specialist Meeting Proceedings, San Francisco, CA, January 2002.

[11] Yeo, H., Bousman, W. G., and Johnson, W., "Performance Analysis of a Utility Helicopter with Standard and Advanced Rotors," Journal of the American Helicopter Society, Vol. 49, No. 3, July 2004.

[12] Yeo, H., and Johnson, W., "Assessment of Comprehensive Analysis Calculation of Structural Loads on Rotors," American Helicopter Society 60th Annual Forum, Baltimore, Maryland, June 2004.

[13] Ormiston, R., "An Investigation of the Mechanical Airloads Problem for Evaluating Rotor Blade Structural Dynamics Analysis," American Helicopter Society 4th Decennial Specialists' Conference on Aeromechanics, San Francisco, CA, January 2004.

Table 1 Rotor Parameters and Operating Conditions

| | H-34 | H-34 | SA 330 | SA 349/2 | UH-60A | BO-105 |
|---|---|---|---|---|---|---|
| Configuration | articulated | articulated | articulated | articulated | articulated | hingeless |
| $N_b$ | 4 | 4 | 4 | 3 | 4 | 4 |
| $\sigma$ | 0.0622 | 0.0622 | 0.091 | 0.0627 | 0.0826 | 0.077 |
| Test | flight | wind tunnel | flight | flight | flight | wind tunnel |
| Radius (in) | 336.0 | 336.0 | 296.7 | 206.7 | 322.0 | 78.7 |
| Scale | full-scale | full-scale | full-scale | full-scale | full-scale | model-scale |
| Low speed | | | | | | |
| $C_T/\sigma$ | 0.075 | | 0.070 | 0.065 | 0.079 | 0.057 |
| $\mu$ | 0.129 | | 0.141 | 0.140 | 0.149 | 0.150 |
| $\alpha_{TPP}$ (deg) | 4.1 | | 1.3 | 1.2 | 0.8 | -4.2 |
| $M_{90,\,tip}$ | 0.628 | | 0.672 | 0.719 | 0.740 | 0.735 |
| High speed | | | | | | |
| $C_T/\sigma$ | | 0.060 | 0.070 | 0.071 | 0.079 | |
| $\mu$ | | 0.390 | 0.362 | 0.361 | 0.368 | |
| $\alpha_{TPP}$ (deg) | | 6.0 | 7.5 | 7.5 | 8.0 | |
| $M_{90,\,tip}$ | | 0.803 | 0.803 | 0.872 | 0.878 | |

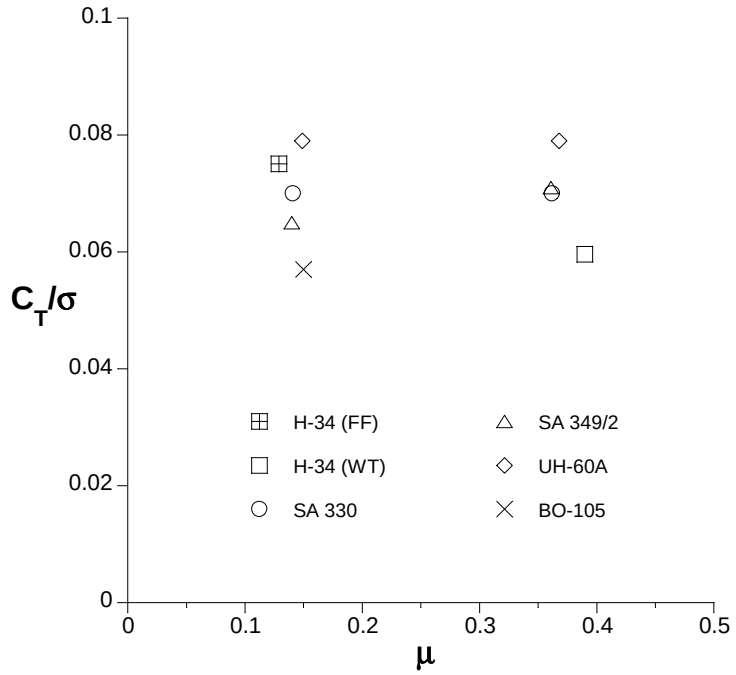


Fig. 1 Rotor thrust coefficient and advance ratio of test data examined

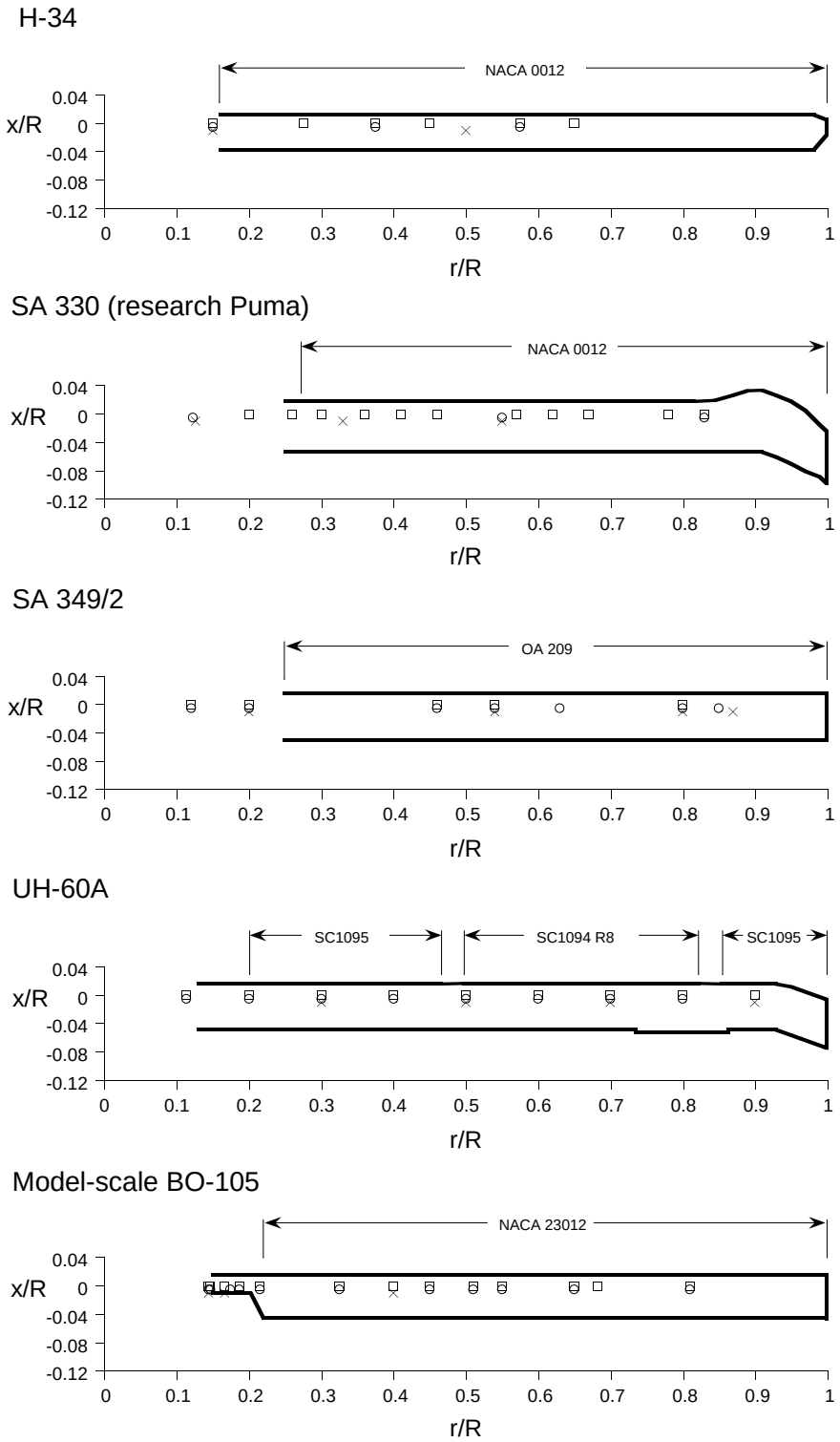


Fig. 2 Blade planforms (□: flap bending, ○: chord bending, and ×: torsion moment measurements)

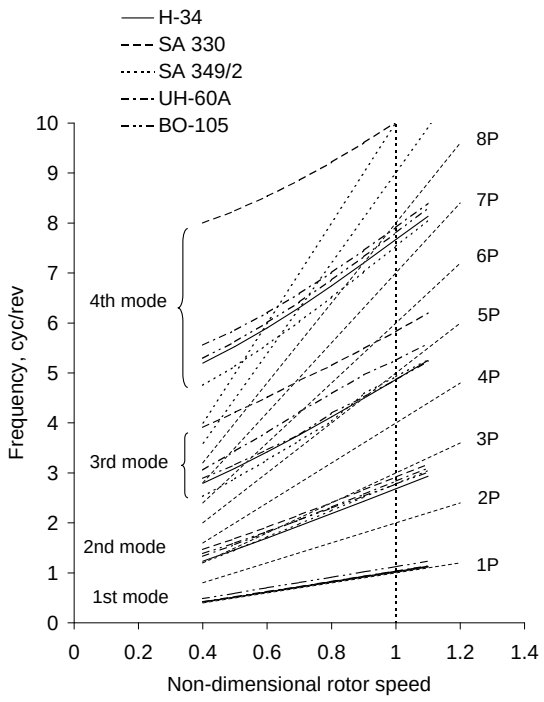


(a) flap mode frequencies

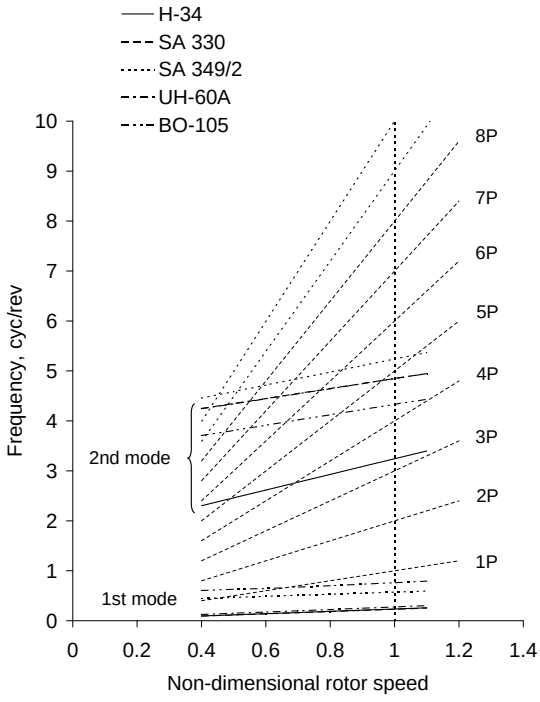


(b) lag mode frequencies

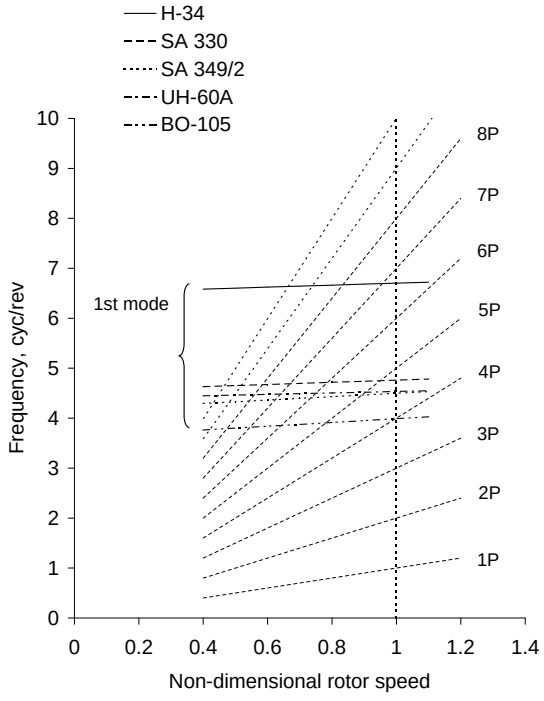


(c) torsion mode frequencies

Fig. 3 Calculated blade frequencies

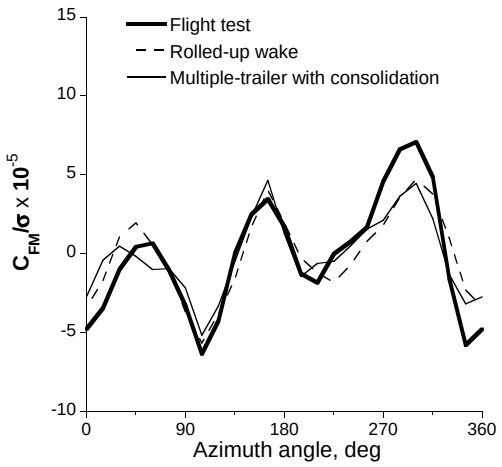


(a) H-34 at $\mu$ = 0.129, r/R = 0.45

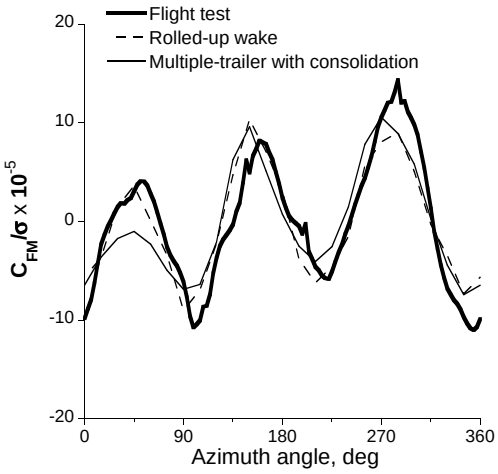


(b) SA 330 at $\mu$ = 0.141, r/R = 0.46

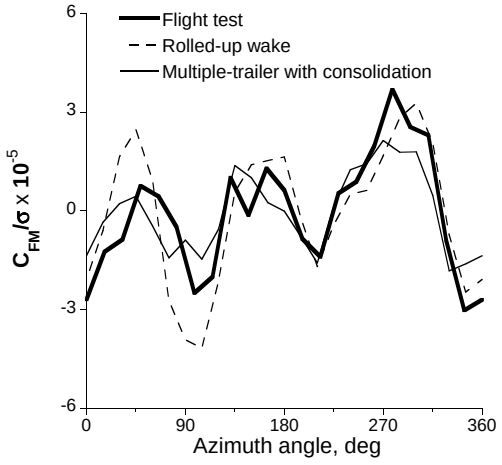


(c) SA 349/2 at $\mu$ = 0.14, r/R = 0.46

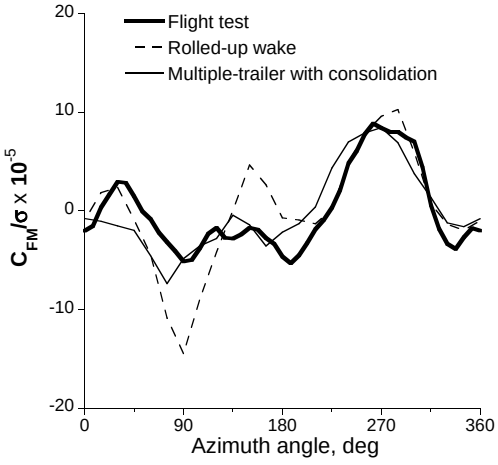


(d) UH-60A at $\mu$ = 0.149, r/R = 0.50

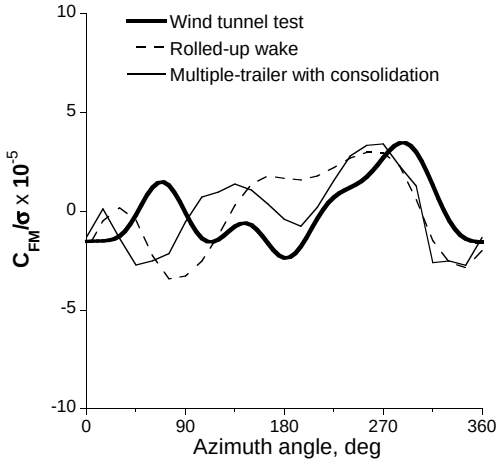


(e) BO-105 at $\mu$ = 0.15, r/R = 0.45

Fig. 4 Calculated and measured blade oscillatory flap bending moment at low speed near r/R = 0.5.

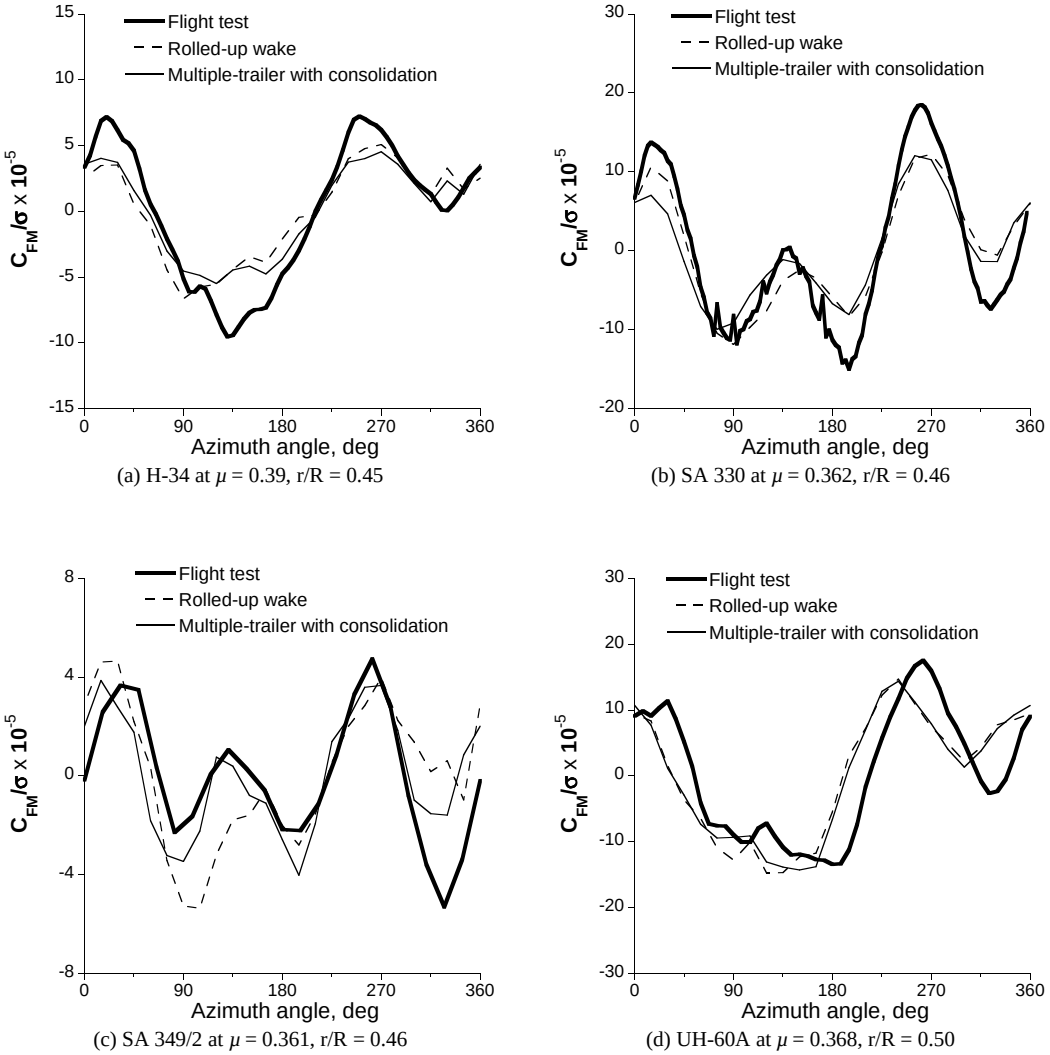


(a) H-34 at $\mu$ = 0.39, r/R = 0.45

(b) SA 330 at $\mu$ = 0.362, r/R = 0.46

(c) SA 349/2 at $\mu$ = 0.361, r/R = 0.46

(d) UH-60A at $\mu$ = 0.368, r/R = 0.50

Fig. 5 Calculated and measured blade oscillatory flap bending moment at high speed near r/R = 0.5.

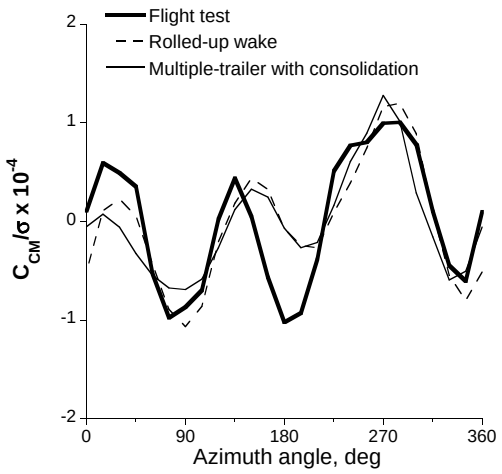


(a) H-34 at $\mu$ = 0.129, r/R = 0.375

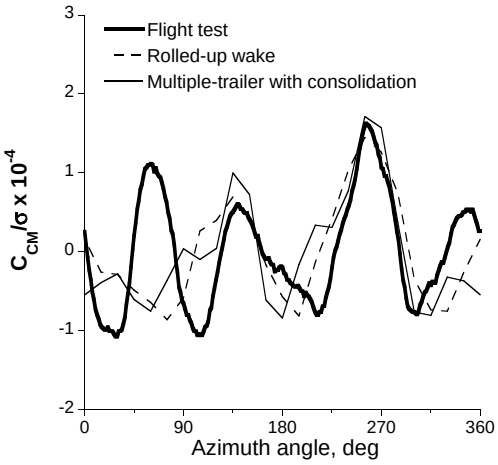


(b) SA 330 at $\mu$ = 0.141, r/R = 0.55

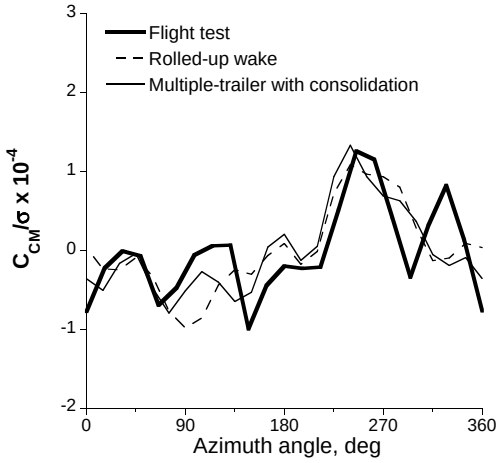


(c) SA 349/2 at $\mu$ = 0.14, r/R = 0.54

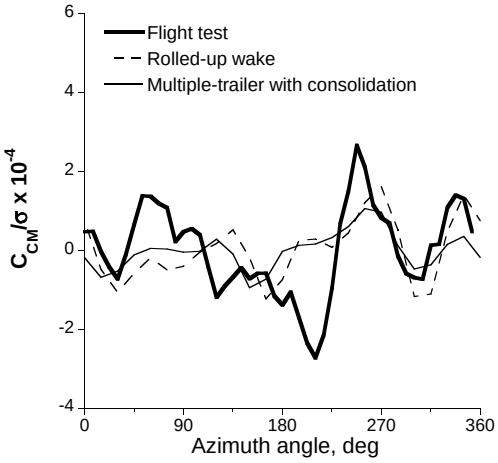


(d) UH-60A at $\mu$ = 0.149, r/R = 0.50

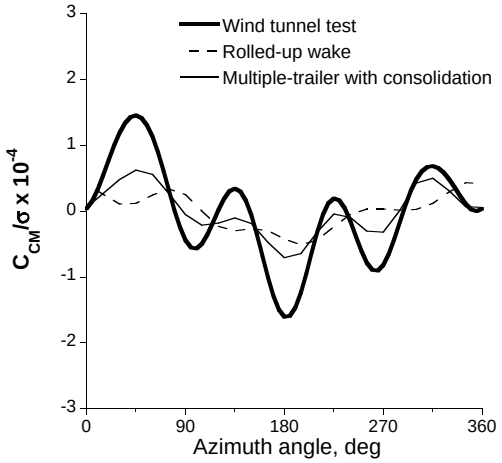


(e) BO-105 at $\mu$ = 0.15, r/R = 0.51

Fig. 6 Calculated and measured blade oscillatory chord bending moment at low speed near r/R = 0.5.

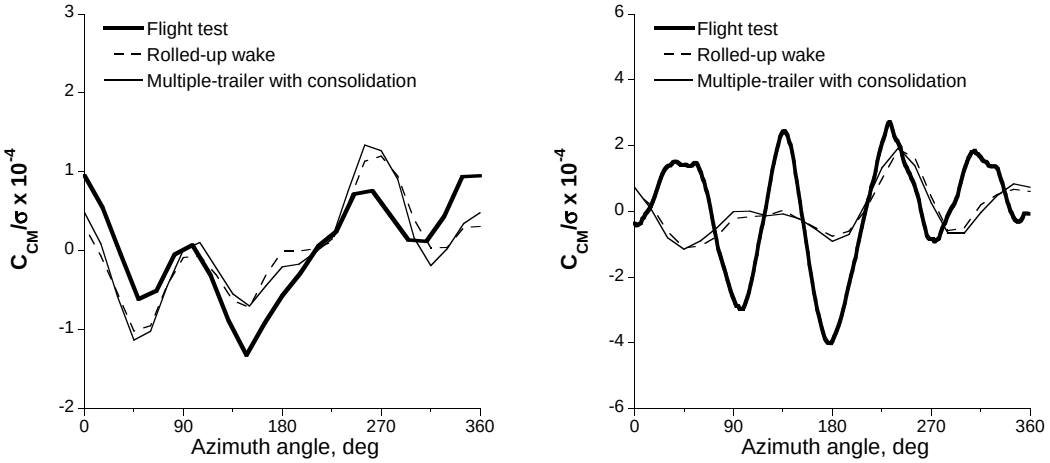


(a) H-34 at $\mu$ = 0.39, r/R = 0.375

(b) SA 330 at $\mu$ = 0.362, r/R = 0.55

(c) SA 349/2 at $\mu$ = 0.361, r/R = 0.54

(d) UH-60A at $\mu$ = 0.368, r/R = 0.50

Fig. 7 Calculated and measured blade oscillatory chord bending moment at high speed near r/R = 0.5.

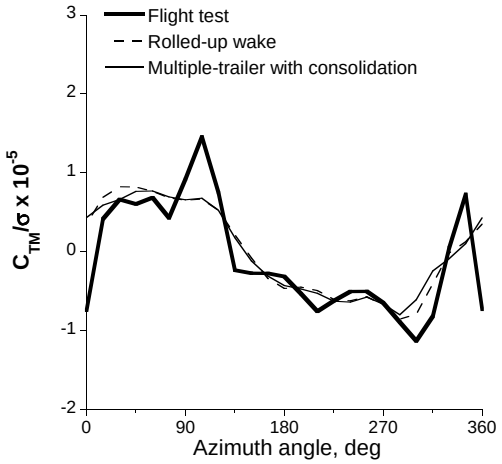


(a) H-34 at $\mu$ = 0.129, r/R = 0.50

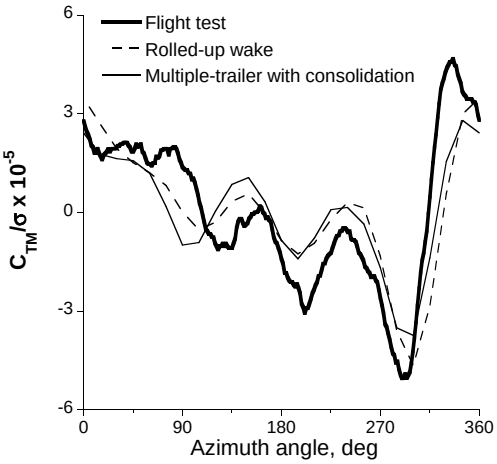


(b) SA 330 at $\mu$ = 0.141, r/R = 0.55

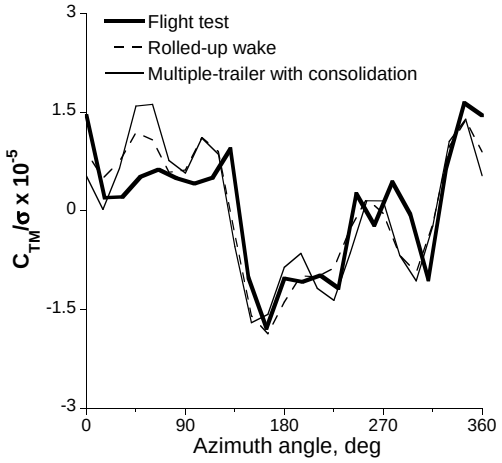


(c) SA 349/2 at $\mu$ = 0.14, r/R = 0.54

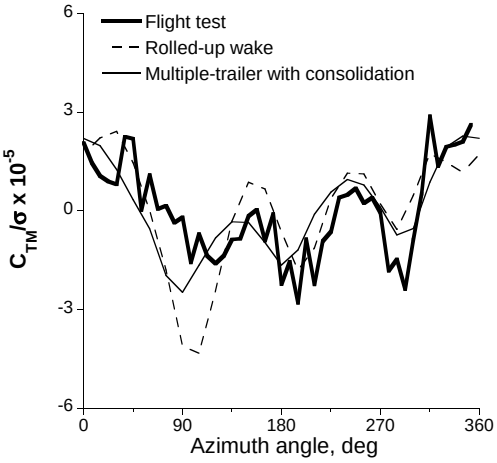


(d) UH-60A at $\mu$ = 0.149, r/R = 0.30

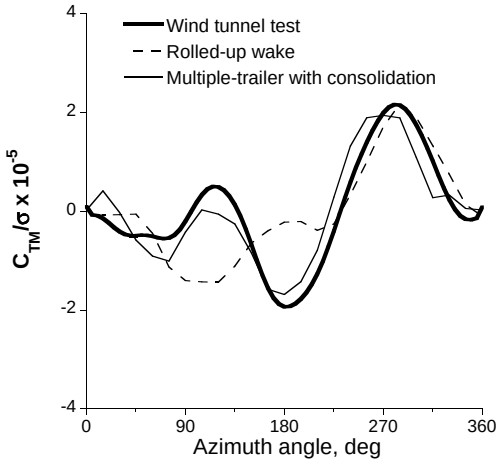


(e) BO-105 at $\mu$ = 0.15, r/R = 0.40

Fig. 8 Calculated and measured blade oscillatory torsion moment at low speed near r/R = 0.5.

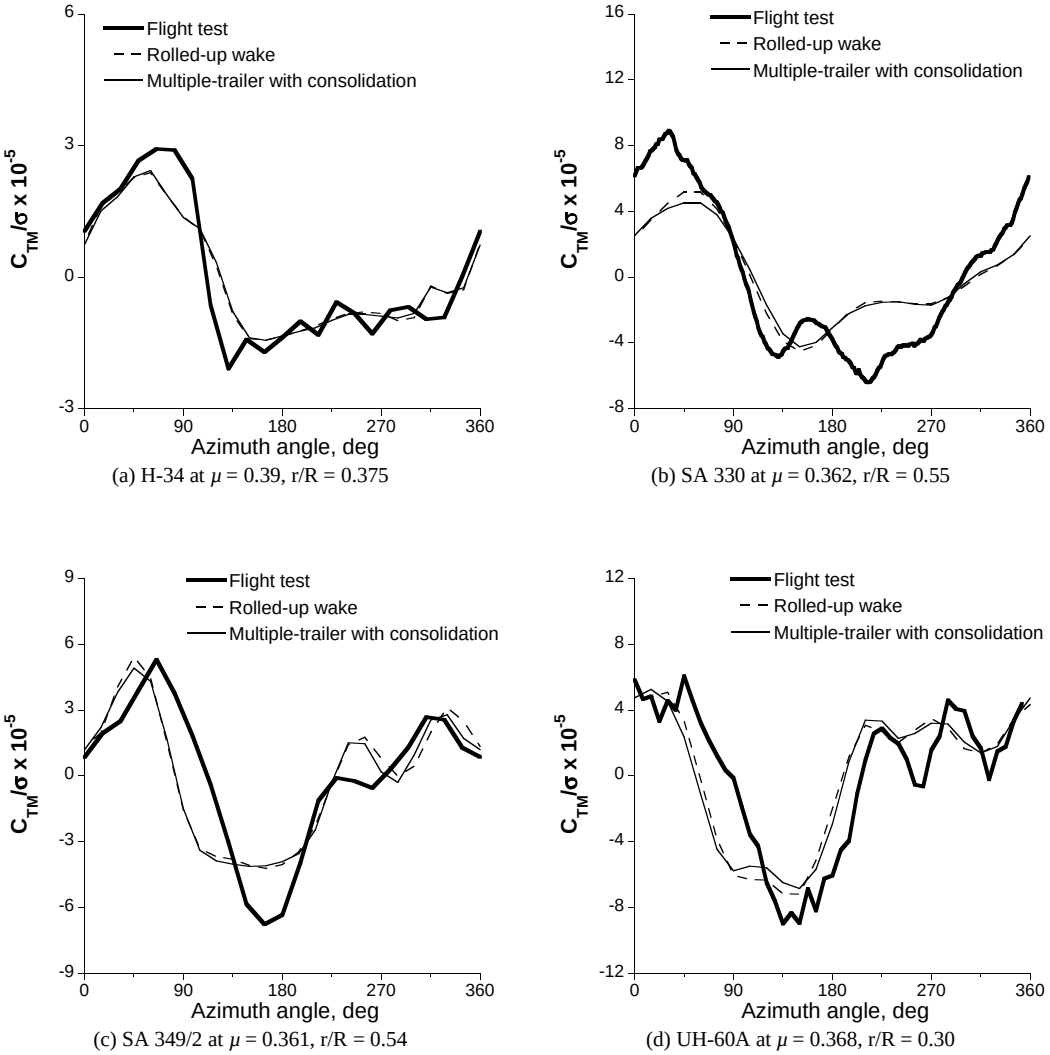


Fig. 9 Calculated and measured blade oscillatory torsion moment at high speed near r/R = 0.5.

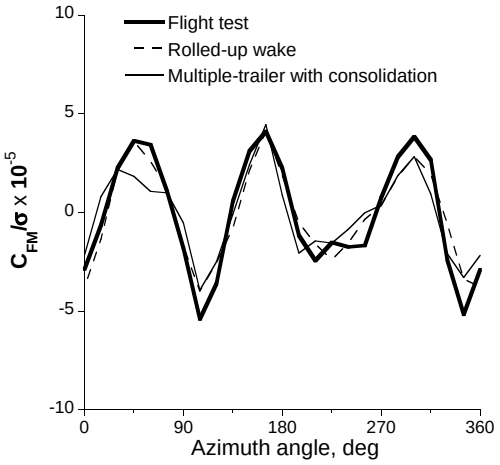


(a) H-34 at $\mu$ = 0.129, r/R = 0.45

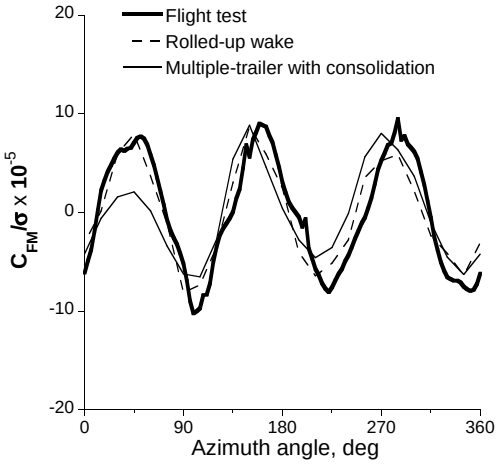


(b) SA 330 at $\mu$ = 0.141, r/R = 0.46

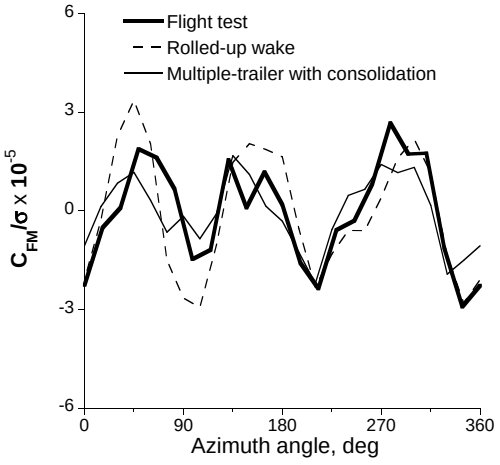


(c) SA 349/2 at $\mu$ = 0.14, r/R = 0.46

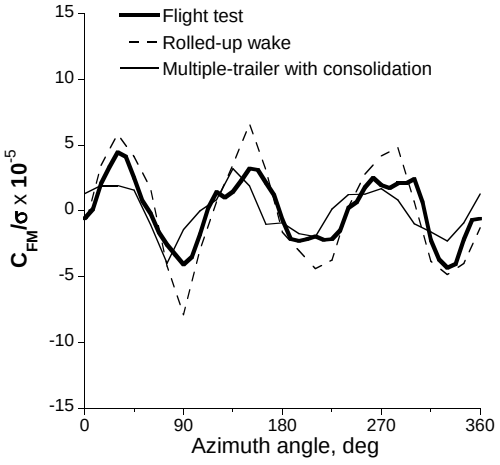


(d) UH-60A at $\mu$ = 0.149, r/R = 0.50

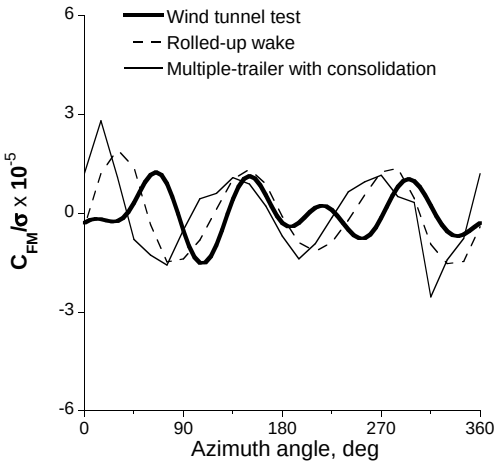


(e) BO-105 at $\mu$ = 0.15, r/R = 0.45

Fig. 10 Calculated and measured blade vibratory flap bending moment at low speed near r/R = 0.5.

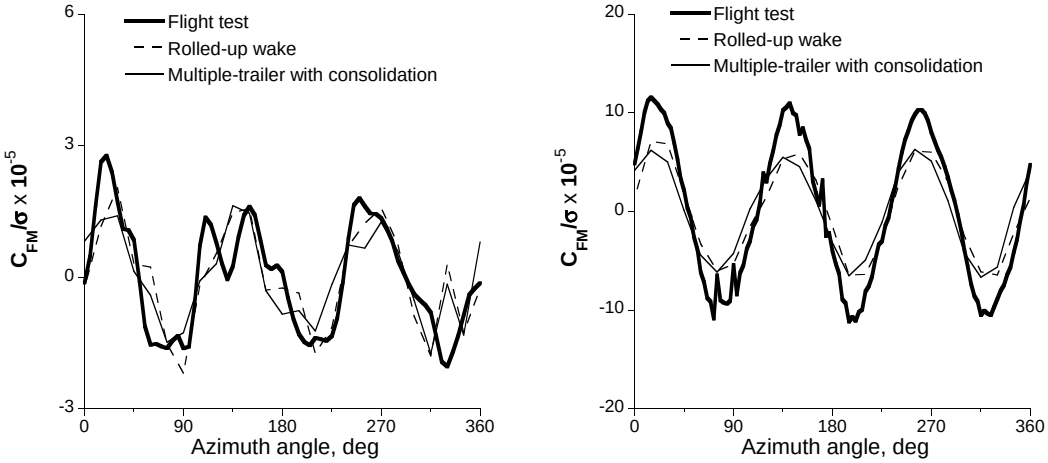


(a) H-34 at $\mu$ = 0.39, r/R = 0.45




(b) SA 330 at $\mu$ = 0.362, r/R = 0.46

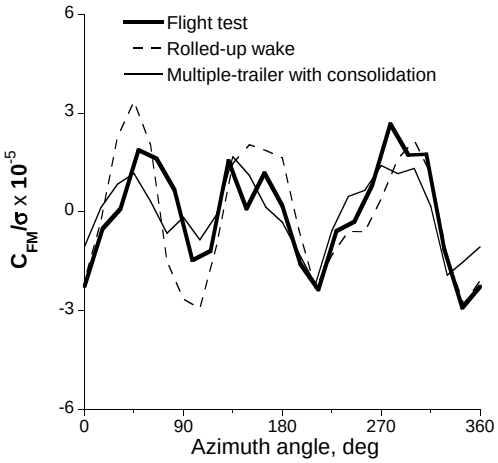


(c) SA 349/2 at $\mu$ = 0.361, r/R = 0.46

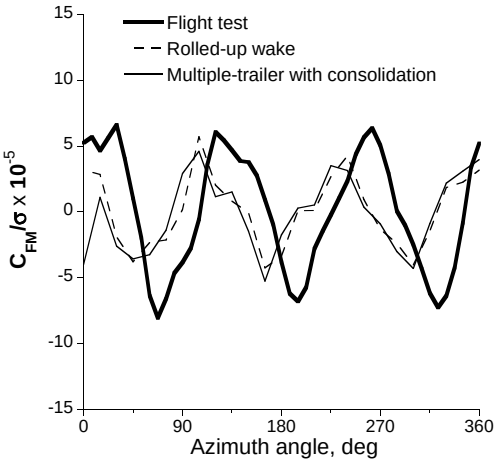


(d) UH-60A at $\mu$ = 0.368, r/R = 0.50

Fig. 11 Calculated and measured blade vibratory flap bending moment at high speed near r/R = 0.5.

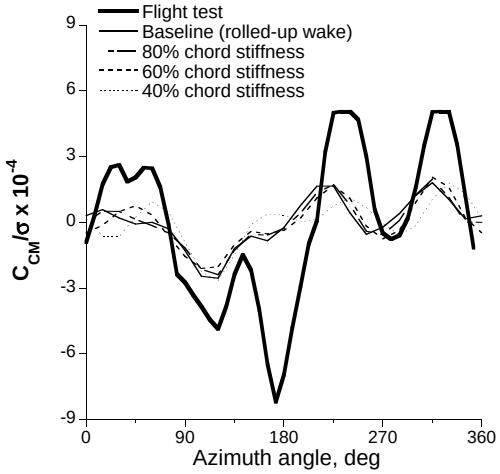


(a) Effect of lag stiffness on the chord bending moment

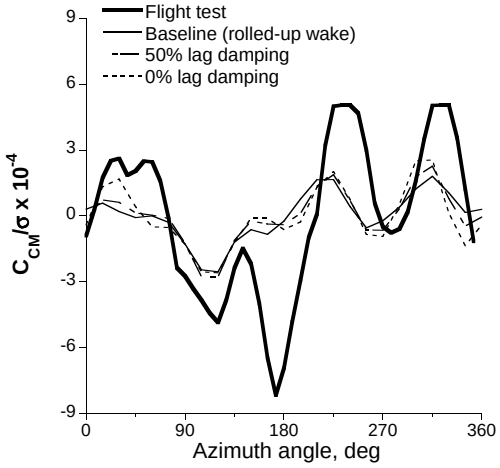


(b) Effect of lag damping on the chord bending moment

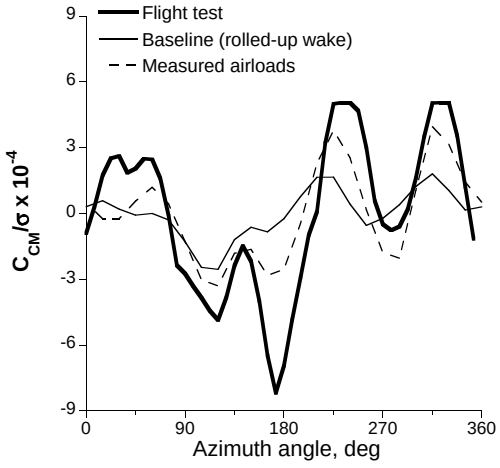


(c) Effect of prescribed measured airloads on the chord bending moment

Fig. 12 Chord bending moment for UH-60A at $\mu$ = 0.368, r/R = 0.50